Ionic Buoyancy Engines: Finite Element Modeling and Experimental Validation

James Akl, Fadi Alladkani, and Barbar Akle*

Abstract

There is a need for buoyancy engines to modulate sensor depth for optimal positioning and station-keeping. Previously, our group developed a highly efficient Ionic Buoyancy Engine that does not have any moving parts and that may be miniaturized. The engine is an osmotic pump triggered by an electric potential change applied to electrodes in an internal closed chamber. This leads to a local reduction in the ionic concentrations near a semi-permeable membrane, which in turn triggers water displacement. In this study a coupled finite element model is used to solve the electrical, chemical, osmotic pressure, and fluid domains. The Nernst-Planck and Poisson equations predict the electro-chemical activities; the osmotic pressure, based on thermodynamic considerations, predicts the pressure across the semi-permeable membrane; and finally, a laminar fluid model is implemented to predict the displacement of water. The model is compared with our previous experimental data, in particular, the effect of the surface area of the electrode and the applied electric potential. In both cases the trends in both models were matching. Finally, the numerical model is used to predict the behavior of the engine due to change in chamber size.

1. Introduction

Undersea distributed networked sensor systems require a miniaturization of platforms and a means of both spatial and temporal persistence. One aspect of this system is the necessity to modulate sensor depth for optimal positioning and station-keeping. Current approaches involve pneumatic bladders or electrolysis; both require mechanical subsystems and consume significant power. For instance, submarines air tanks are filled with sea water for sinking while purged using pressurized air to float vessel. Divers' BCD (Buoyancy Control Device) implements a similar concept by inflating bags of air, thus the density is manipulated by volume increase at constant mass. A recent design [1] implemented an IPMC transducer as a high surface area electrode for a low power buoyancy engine. Electrolysis at the IPMC electrodes generates hydrogen and oxygen gas which replace the water in the gas chamber resulting in the floatation of the engine. The WET engine is a similar device that uses conventional electrolysis techniques [2].

Recently [3] presented a novel biologically inspired highly efficient buoyancy engine. The engine relies on ionic motion and osmotic pressures to displace a water from the ocean into and out of the buoyancy engine. The engines inner chamber volume is held constant by having it enclosed in rigid walls. The displaced water will alter the mass and hence the buoyancy leading to either sinking or floating. The engine is composed of an enclosure with an opening to the ocean that is sealed by a Nafion ionomer membrane. Internally the design has a flexible membrane separating the water from a gas enclosure which expands and contracts upon the diffusion of water. Two electrodes are placed on the inside of the enclosure. The semi-permeable membrane Nafion allows water motion in and out of the enclosure while blocking anions from being transferred. The two electrodes generate local concentration changes of ions upon the application of an electrical field; these changes lead to osmotic pressures and hence the transfer of water through the semi-permeable membrane.

* barbar.akle@lau.edu.lb — Phone +961 9 547 262 — Fax +961 9 546262 — www.lau.edu.lb

In this study a coupled finite element model is used to solve the electrical, chemical, osmotic pressure, and fluid domains. The Nernst-Planck and Poisson equations predict the electro-chemical activities; the osmotic pressure, based on thermodynamic considerations, predicts the pressure across the semi-permeable membrane; and finally, a laminar fluid model is implemented to predict the displacement of water. The model is compared with our previous experimental data, in particular, the effect of the surface area of the electrode and the applied electric potential. In both cases the trends in both models were matching. Finally, the numerical model is used to predict the behavior of the engine due to change in chamber size.

This paper is organized as follows: section 2 describes the numerical model and the parameters used in the Finite Element simulation. The numerical results are compared to the previous experimental results in section 3, and finally section 4 concludes the study.

2. Modeling considerations

The finite element method (FEM) model is formulated and simulated on COMSOL 5.4. All time-dependent vector fields are modeled in the two-dimensional Euclidean space $\mathbb{R}^2$.

Electrical field

The chemical and electrical fields are coupled via the Poisson equation, which models the electric potential at the electrodes.

$$\nabla^2\Psi = -\frac{F}{\epsilon_0\epsilon_r}\sum_j z_j c_j \tag{1}$$

It is obtained by combining the Helmholtz ($\mathbf{E} = \nabla\Psi$), Gauss ($\nabla \cdot \mathbf{D} = \rho_\Psi$), and material ($\mathbf{D} = \epsilon_0\epsilon_r\mathbf{E}$) laws. Ψ is the electric potential, $\mathbf{E}$ the electric field tensor, $\mathbf{D}$ the dielectric displacement tensor, ρ_Ψ the volumetric charge density, ϵ_0 the permittivity of empty space, ϵ_r the material dielectric constant, $F \approx 96485.3\ \mathrm{C}\cdot\mathrm{mol}^{-1}$ Faraday's Constant, c_j the concentration fields and z_j the valence of each species j. The coupling essentially occurs with the equality $\rho_\Psi = F\sum_j z_j c_j$.

Chemical field

The transport of diluted ionic species is modeled by the time-dependent and first-order Nernst-Planck equation.

$$\dot{c}_j = \nabla \cdot \left(D_j \nabla c_j\right) + R_j \tag{2}$$

Since there is no ionic displacement between the inside and outside of the chamber, the source terms $R_j = 0$ for every species j. Where D_j denotes the diffusion coefficients of every species j. The diffusion coefficients are assumed to be isotropic.

Osmotic pressure

The chemical field and osmotic pressure are then coupled using the thermodynamic considerations of the solution.

$$\pi = RT\sum_j c_j i \tag{3}$$

Where π is the osmotic pressure field, R the ideal gas constant, T the temperature, and i the van t'Hoff factor.

Fluid displacement field

The osmotic pressure and fluid flow across the ionomer membrane are then coupled using the Navier-Stokes equations, used to model laminar fluid flow. Since water is considered, the fluid is assumed to be incompressible.

$$\rho(\dot{\mathbf{u}} + \mathbf{u} \cdot \nabla \mathbf{u}) = \nabla \cdot \left[\mu\left(\nabla \mathbf{u} + (\nabla \mathbf{u})^{\mathrm{T}}\right) - p\mathbf{I}\right] + \mathbf{F} \tag{4}$$

Where ρ is the fluid mass density, $\mathbf{u}$ the fluid velocity field, p the fluid pressure, μ the dynamic viscosity, $\mathbf{I}$ is the identity matrix, and $\mathbf{F} = \nabla\pi$ the external source.

Discretization

The model uses triangular shell elements in linear concentration and velocity fields. All discretized fields are real-valued. Since the simulation reaches nanoscale, adaptive meshing is used for performance optimization as seen in Fig. 1. The mesh becomes finer near the electrodes and coarser near fluid areas of low interest. The mesh size at the electrodes reaches 0.1 nm.

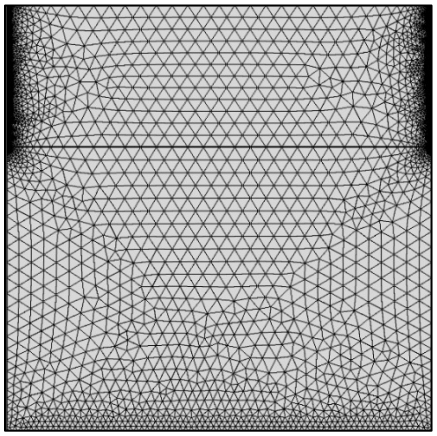

Figure 1. Discretization of the buoyancy engine and outside medium using an adaptive mesh.

Parameters

All parameters used in the finite element model are summarized below in Table 1.

Initial and Boundary Conditions

As Shown in the setup in Figure 2, there are four initial conditions: 1. zero initial electric potential ($\Psi = 0$), 2. zero initial fluid velocity ($\mathbf{u} = \mathbf{0}$), 3. zero initial gauge pressure ($p = 0$), and 4. equal initial ion concentrations ($c_1 = c_2 = c_i$).

As for boundary conditions, the cathode and anode respectively have constant electric potentials of $\Psi = V_0$ and $\Psi = -V_0$. At the walls, there are no-slip ($\mathbf{u} = \mathbf{0}$), zero-charge ($\mathbf{n} \cdot \mathbf{D} = 0$), and zero-ion flux ($-\mathbf{n} \cdot \mathbf{N}_i$) boundary conditions. At the top, there is an open boundary condition $\left(\left[\mu\left(\nabla \mathbf{u} + (\nabla \mathbf{u})^{\mathrm{T}}\right) - p\mathbf{I}\right]\mathbf{n} = 0\right)$ to simulate an open ocean. Finally, at the ionomer membrane,

there exists a normal total flux boundary condition ($D_i \nabla c_i \cdot \mathbf{n} = 0$) and a specified pressure $p_0 = 2\, ic_i RT$. Below is provided Fig. 2 to locate and summarize the boundary conditions.

Table 1
Geometric dimensions and physical properties of the buoyancy engine and surrounding medium.

Parameter	Variable	Value
Engine width	w	1.0 μm
Engine height	H	1.0 μm
Electrode height	h_e	0.2 μm
Diffusion constant	D_w	10^{-5} m²/s
Initial concentration	c_i	0.01 mol/m³
Water density	ρ_w	1023 kg/m³
Water viscosity	μ_w	0.00188 Pa·s
Van t' Hofft factor	i	1
Ideal gas constant	R	8.314472 $J \cdot K^{-1} \cdot mol^{-1}$
Electrode voltage	V	0.01 V
Temperature	T	293.15 K
Faraday's constant	F	96485 C/mol
Relative permittivity	ϵ_w	80

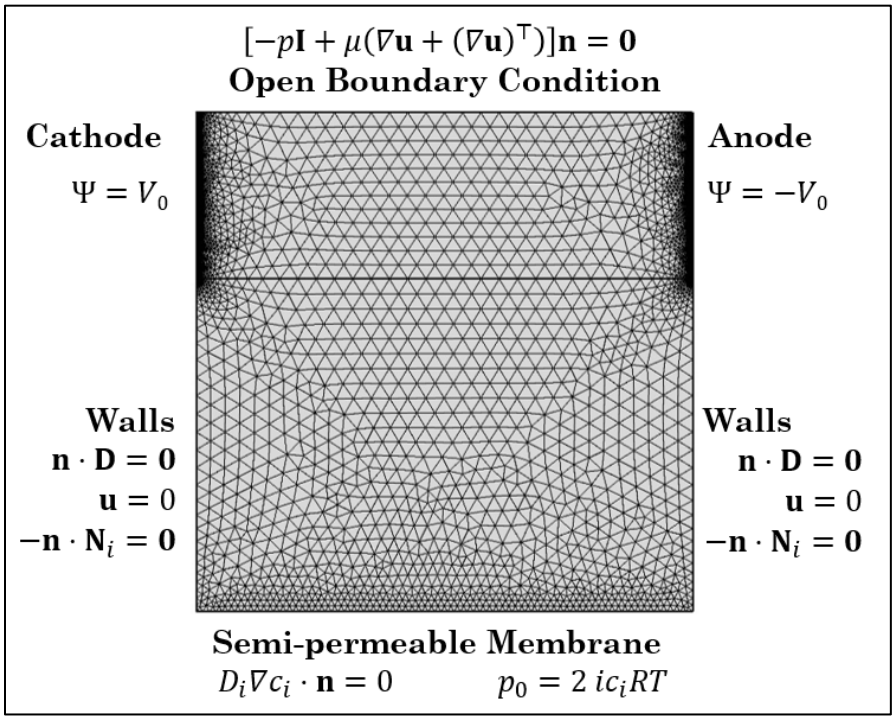

Figure 2. Boundary conditions at and across the various buoyancy engine elements.

3. Numerical Results

The finite element method (FEM) model is first calibrated in 1D and 2D against known data in Literature [4][5]. Later the model is simulated and the electrochemical behavior is observed. Finally, the numerical results are compared to experimental measurements.

Electrochemical simulation

The chemical and electrical fields are coupled via the Poisson equation, which models the electric potential at the electrodes. The ionic concentrations are calculated and plotted across three positions across the engine as seen in Fig. 3. The data demonstrates that a normal electric double layer is emerging between the two electrodes, the ionic concentration change drops significantly as expected when moving further away from the electric field toward the bottom of the engine. Most importantly, the numerical simulations demonstrate a drop in the average ionic concentration right at the semipermeable membrane (Nafion) as it could be seen in the lower plot in Fig. 3.

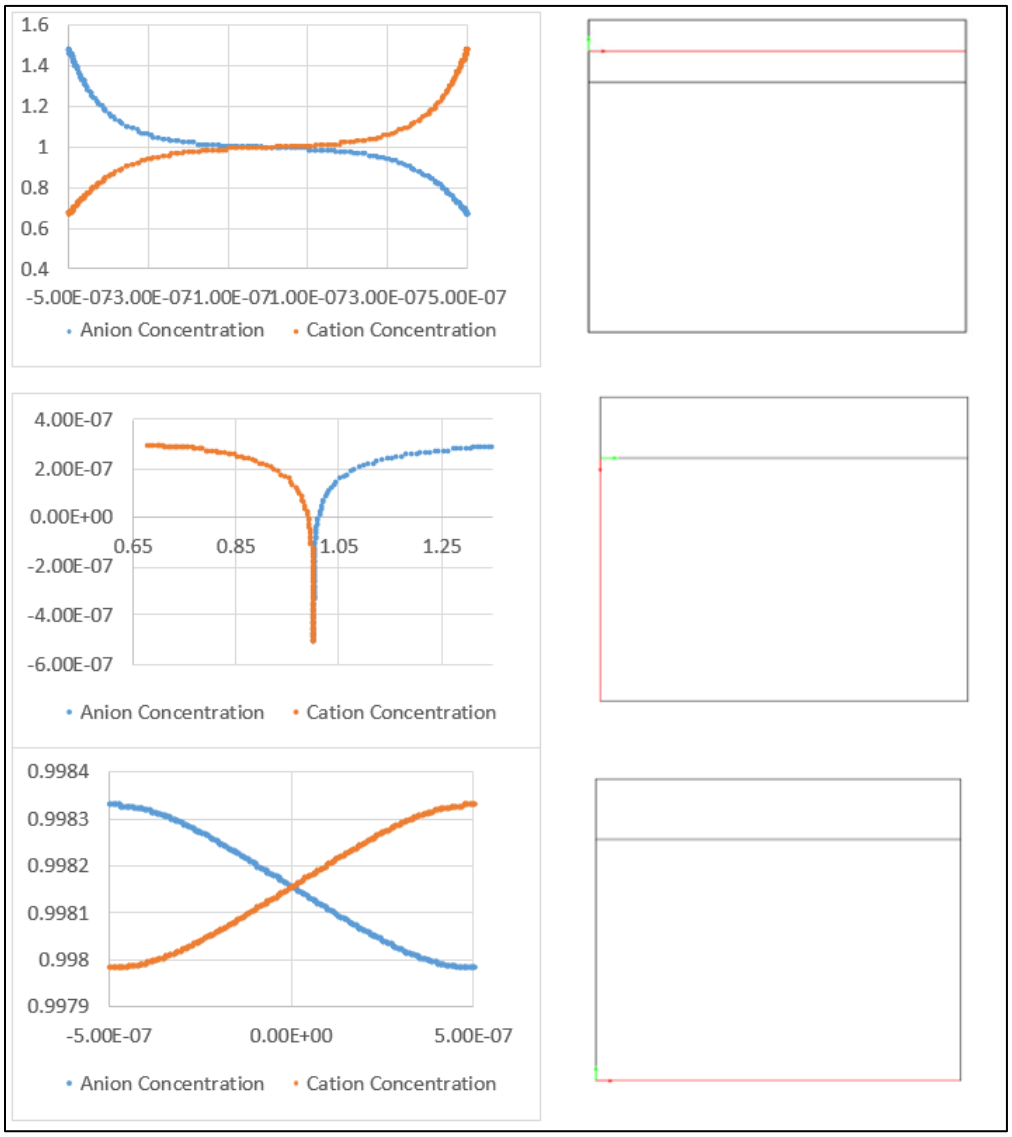

Figure 3. The relative ionic concentration at different locations of the buoyancy engine.

Comparing Numerical and Experimental Results

The average ionic concentration at the Semi-permeable membrane is computed and correlated to the amount of fluid displaced. A lower concentration leads to a higher osmotic pressure difference across the membrane which in turn displace more water through the semipermeable membrane. Fig. 4 top, shows that the average concentration as a function of electrode surface area (parameter length) decreases with increasing length. This anticipate a larger fluid displaced which correlates well with the experimental data (Fig. 4, top right) [6]. Furthermore, increasing the applied potential results in a significantly lower average ionic concentration which has a significant effect on the water displaced as it could be seen in experimental results (Fig. 4, bottom right).

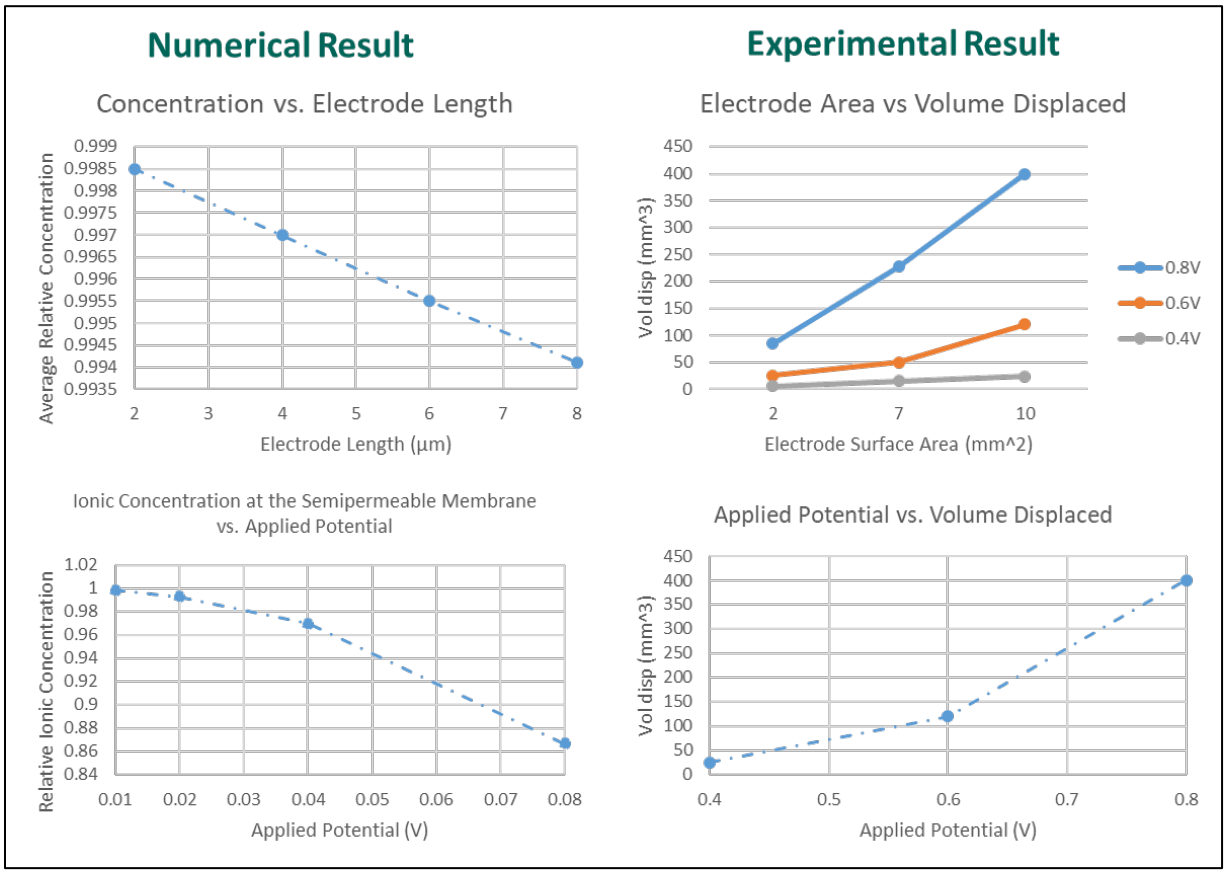

Figure 4. Numerical results compared to the experimental results for the variation in electrode surface area and in the applied potential.

4. Conclusion

A coupled electro-chemo-mechanical model is developed based on the Nernst-Plank, Poisson, thermodynamics, and Navier-Stokes equations is developed and solved using finite element methods. The model is first calibrated with previous similar results, and later used to calculate trends in the electro-chemical fields. These trends demonstrated that the ionic concentration at the semi-permeable membrane is reduced when an electric potential is applied across the electrodes. This lead to the rise of osmotic pressures, resulting in fluid flow across the membrane. Trends from the model are successfully compared to the experimental results obtained earlier by our group. These trends indicate that a larger electrode or a larger applied potential will lead to bigger amount of fluid displaced.

5. Acknowledgement

The authors would like to acknowledge the support of the Lebanese American University School of Engineering Research Council for partial financial Support.

6. References

[1] U.S. Food and Drug Administration (FDA), 2012.

[2] S. Angeli, D. Yan, F. Telischi, T. J. Balkany, X. M. Ouyang, L. L. Du, A. Eshraghi, L. Goodwin, X. Z. Liu, "Etiologic diagnosis of sensorineural hearing loss in adults", Otolaryngol Head Neck Surg June 2005 vol. 132 no. 6 890-895

[3] B. Akle, W. Habchi, R. Abdelnour, J. Blottman, D. Leo, “Biologically inspired highly efficient buoyancy engine”, Proceedings of the SPIE 19th Annual Symposium on Smart Structures and Materials, San Diego, California, Volume 833, 201.

[4] T. Wallmersperger, B. Akle, D.J. Leo, B. Kröplin “Electromechanical Response in Ionic Polymer Transducers: An Experimental and Theoretical Study”, Composite Science and Technology 68(5), S. 1173-1180, 2008

[5] B. Akle, W. Habchi, T. Wallmersperger, E. Akle and D. Leo, “High surface area electrodes in ionic polymer transducers: numerical and experimental investigations of the electro-chemical behavior” Journal of Applied Physics, 109(7), 074509, 2011.

[6] B. Akle, J. Nasser; A. Hijazi,” Modeling and experimentally characterizing ionic buoyancy engines”, Proceedings of the SPIE 24th Annual Symposium on Smart Structures and Materials, Seattle, Washington, Volume 10163, 2017.